UCLA
COMPUTATIONAL AND APPLIED MATHEMATICS

Studies on Error Propagation for Certain Nonlinear Approximations to Hyperbolic Equations: Discontinuities in Derivatives

Rosa Donat

August 1992

CAM Report 92-36

Department of Mathematics
University of California, Los Angeles
Los Angeles, CA. 90024-1555

Studies on Error Propagation for certain Nonlinear Approximations to Hyperbolic Equations: Discontinuities in Derivatives.

Rosa Donat

August 17, 1992

Abstract

The accuracy of numerical approximations to piecewise smooth solutions of hyperbolic partial differential equations is greatly influenced by the presence of singularities in the solution. In the presence of coupling (through lower order terms or variable coefficients), high order numerical approximations can lose accuracy in large regions, where the analytical solution is known to be smooth, due to the spreading of the errors that the singularities introduce in the computation.

This phenomenon, which has been analyzed in the past fifteen years for a number of classical linear methods, is studied here for numerical approximations obtained with nonlinear ENO schemes. The study of the *local* rate of convergence allows us to identify the necessary techniques to reduce the spread of errors and to avoid the accuracy loss of the computed approximations.

The techniques we develop, can be applied to nonlinear hyperbolic partial differential equations and systems to sharpen the resolution of corners of rarefaction waves.

1 Introduction

At a point where the solution of a hyperbolic problem has a jump discontinuity or a discontinuity in one of its derivatives, the differential equation

*Research supported in part by ONR Grant N00014-86-K-0691 and DGICYT PS90-0265

ceases to be valid, and special techniques must be used to guarantee that numerical approximations to the solution stay accurate.

For linear schemes, the phenomenon of the loss of accuracy caused by singularities in the solution of a hyperbolic problem has been studied during the past fifteen years. In [10], Majda and Osher realize that the loss of accuracy on linear dissipative approximations to a model hyperbolic system does not remain confined to a close neighborhood of the characteristics. In the presence of coupling (through variable coefficients or lower order terms) the rate of convergence in the region of influence of the singularity drops down to first order, independently of the order of the underlying scheme. Similar studies were conducted by Majda, Osher and McDonough ([9]) for spectral methods. The conclusion, in both cases, was that some sort of preprocessing of the initial data is necessary if one wants an accurate numerical approximation at all regions where the analytical solution is smooth.

Recently, a great deal of attention has been devoted to the study of nonlinear methods for the numerical solution of hyperbolic problems. Among these, ENO (Essentially Non Oscillatory [6, 7, 13]) schemes have some very desirable properties: They are highly accurate in smooth regions and they avoid spurious oscillations around discontinuities (without having to resort to parameter-tuned artificial viscosity terms); shock profiles are very sharp, but contact discontinuities are smeared over a relatively large number of cells.

In [1], we analyzed the effect of coupling in the accuracy of numerical approximations computed with ENO methods of various degrees of accuracy. As in the case of linear schemes, we found that, in the presence of coupling, the computed solution becomes only first order accurate in the region of influence of a singularity (a jump or a discontinuity in the derivative), regardless of the order of the underlying ENO scheme. With an eye on the error spread introduced in the computation by a contact discontinuity as the cause of the accuracy loss, we turned to the two existing techniques designed to reduce this error spread: Artificial Compression [3, 14] and Subcell Resolution [5]. As expected, only the Subcell Resolution (SR) technique was able to raise the accuracy to second order (see [1] for details). In the example under investigation, we were unable to obtain better accuracy rates, the reason being the discontinuities in derivatives, which we will call *corners* from now on, developed by the solution. In an attempt to better understand the phenomenon as well as to improve the accuracy of numerical approximations obtained via ENO methods, we continue studying the phenomenon of propagation of error into regions of smoothness. In this paper we shall

concentrate on the analysis of the error spread introduced by a corner in numerical computations with ENO methods, and we shall devise a technique, based on Harten's Subcell Resolution, that is able to eliminate it.

The rest of the paper is organized as follows: Section 2 describes, for the sake of completeness, the basic ideas of ENO schemes and the original SR technique due to Harten. Section 3 presents a computational analysis of the error spread introduced in the computation by a corner and highlights the main sources of trouble in a straightforward application of Harten's SR. Section 4 describes and analyzes a corrected form of the SR technique that works suitably for corners. Section 5 contains examples of applications to systems of conservation laws and some conclusions.

2 An overview of ENO schemes; Harten's Subcell Resolution

In this section we shall review the underlying principles of ENO schemes and of the original Subcell Resolution technique due to Harten.

Consider, for simplicity, the one dimensional case, and let us denote by $E(t)$ the exact evolution operator for the conservation law, i.e., the solution $u(x,t)$ satisfies

$$u(x,t) = E(t-t_0)u(x,t_0).$$

Given a spatial step-size h, we define the *sliding average* of $u(x,t)$ as

$$\bar{u}(x,t) = \frac{1}{h}\int_{-h/2}^{h/2} u(x+y,t)dy \equiv (A_h \cdot u)(x,t).$$

The evolution operator for the sliding average will thus be

$$\bar{u}(x,t) = (A_h \cdot E(t-t_0))u(x,t_0).$$

To specify a method, we have to define its discrete evolution operator $\bar{E}(\tau)$, where τ is the time step of the discretization, i.e.,

$$\bar{u}^{n+1} = \bar{E}(\tau)\cdot\bar{u}^n.$$

The abstract form of an ENO scheme has

$$\bar{E}(\tau)\cdot\bar{u} = A_h \cdot E(\tau)\cdot R(\cdot,\bar{u}), \tag{1}$$

where $R(\cdot,\bar{u})$ is a piecewise polynomial reconstruction of u from its cell averages $\bar{u}$.

It turns out that this scheme can be written in standard conservation form and, therefore, bounded limits as $h \to 0$ of approximate solutions converge to weak solutions of the conservation law [6, 7].

ENO schemes call for $R(x;\bar{u})$, a nonoscillatory reconstruction of u from its cell averages. In fact, the most important step in an ENO scheme is the reconstruction step. Given $\{v_j^n\}$ which are approximations to $\{\bar{u}_j^n\}$, the cell averages of the true solution, we must extract high order accurate pointwise information to solve the reconstruction problem without introducing $O(1)$ Gibbs-like spurious oscillations near the discontinuities. The reconstruction algorithm is derived from an interpolation technique that uses an adaptive stencil of grid points. Consequently, the resulting scheme is highly nonlinear, even when applied to a linear equation.

For an rth order accurate method, $R(x;\bar{u})$ is a piecewise polynomial function of x, of uniform polynomial degree $r-1$, that satisfies

$$R(x;\bar{u}) = u(x) + e(x)h^r + O(h^{r+1}) \tag{2}$$

at all points x for which there is a neighborhood where u is smooth.

In [6, 7], two different approaches to the design of $R(x,\bar{u})$ are considered:

- RP: Reconstruction via the Primitive Function.
- RD: Reconstruction via Deconvolution.

We refer to [6, 7] for specific details on these two methods. Here we will only describe the main features relevant to our discussion.

(1) *Reconstruction via the Primitive function.*

Given the cell averages, $\bar{w}_j$, of a piecewise smooth function $w(x)$

$$\bar{w}_j = \frac{1}{h_j}\int_{x_{j-\frac{1}{2}}}^{x_{j+\frac{1}{2}}} w(y)dy, \qquad h_j = x_{j+\frac{1}{2}} - x_{j-\frac{1}{2}},$$

we can immediately evaluate the point values of the primitive function $H(x)$

$$H(x) = \int_{x_0}^{x} w(y)dy$$

by

$$H(x_{j+\frac{1}{2}}) = \sum_{i=i_0}^{j} h_i \bar{w}_i.$$

Let $Q_r(x;H)$ be a piecewise polynomial function satisfying

$$Q_r(x_{j+\frac{1}{2}}) = H(x_{j+\frac{1}{2}}) \qquad \forall\ j,$$

$$\frac{d^l}{dx^l}Q_r(x;H) = \frac{d^l}{dx^l}H(x) + O(h^{r-l+1}) \qquad 0 \le l \le r \qquad (3)$$

in smooth regions. Since

$$w(x) = \frac{d}{dx}H(x),$$

the reconstruction for w is obtained as

$$R(x;\bar{w}) = \frac{d}{dx}Q_r(x;H).$$

(2) *Reconstruction via Deconvolution*

Assume now that the mesh is uniform and consider the given cell averages $\bar{w}_j$ to be the point values of $\bar{w}(x)$, the globally defined sliding-average function of w, i.e.

$$\bar{w}_j = \bar{w}(x_j)$$

where

$$\bar{w}(x) = \frac{1}{h}\int_{-h/2}^{h/2} w(x+y)dy.$$

We then proceed to construct a piecewise polynomial function, which we also call $Q_r(x;\bar{w})$, that interpolates $\bar{w}$ at the x_j for each j. We ask again that

$$Q_r(x_{j+\frac{1}{2}}) = \bar{w}(x_{j+\frac{1}{2}}) \qquad \forall\ j,$$

$$\frac{d^l}{dx^l}Q_r(x \pm 0;\bar{w}) = \frac{d^l}{dx^l}\bar{w}(x) + O(h^{r-l+1}) \qquad 0 \le l \le r. \qquad (4)$$

in regions of smoothness.

Defining

$$\bar{D}_{0,j} = \quad \bar{w}_j$$

$$\bar{D}_{l,j} = \quad h^l \mathrm{mmod}(\frac{d^l}{dx^l}Q_r(x_j - 0;\bar{w}), \frac{d^l}{dx^l}Q_r(x_j + 0;\bar{w})) \qquad for \quad 1 \le l \le r-1,$$

where $\mathrm{mmod}(x,y)$ is the min mod function

$$\mathrm{mmod}(x,y) = \begin{cases} s \cdot \min(|x|,|y|) & \text{if } \mathrm{sgn}(x) = \mathrm{sgn}(y) = s \\ 0 & \text{otherwise,} \end{cases}$$

we can easily check that

$$\bar{D}_{l,j} = h^l \bar{w}(x_j) + O(h^r); \tag{5}$$

Then, since

$$\bar{w}(x) = (w * \psi_h)(x)$$

$$\psi_h = \begin{cases} 1/h & \text{for} |x| < h/2 \\ 0 & \text{for} |x| > h/2 \end{cases}$$

we can calculate $(D_{0,j}, \cdots D_{r-1,j})$ such that

$$D_{k,j} \approx h^k w^{(k)}(x_j) \qquad 1 \leq k \leq r$$

by a deconvolution procedure to $O(h^r)$ (see [7]).

The reconstruction is then defined as

$$R(x, \bar{w}) = \sum_{k=0}^{r-1} \frac{1}{k!} D_{k,j}[(x - x_j)/h]^k \qquad \text{for} \quad |x - x_j| < h/2.$$

In each case, the approximation properties of $R(x; \bar{w})$ at a particular cell are derived directly from (3) or (4).

Let us concentrate now on the RP reconstruction. Q_r satisfies

$$Q_r(x; H) = q_j^{(r)}(x) \qquad \text{for} \quad x_{j-\frac{1}{2}} \leq x \leq x_{j+\frac{1}{2}}$$

where $q_j^{(r)}(x)$ is the unique polynomial of degree r that interpolates H at the $r+1$ points

$$S_r(j) = \{x_{i_r(j)}, \cdots, x_{i_r(j)+r}\}$$

for a particular choice of $i_r(j)$ (to be described later). Choosing j such that

$$j - r + \frac{1}{2} \leq i_r(j) \leq j - \frac{1}{2}$$

ensures that

$$q_j(x_{j-\frac{1}{2}}) = H(x_{j-\frac{1}{2}}), \qquad q_j(x_{j+\frac{1}{2}}) = H(x_{j+\frac{1}{2}}).$$

It is now obvious that (3) will only be satisfied if the set $S_r(j)$, the stencil of points assigned to the jth cell, lies *entirely* in a smooth region of w.

A similar argument shows that the same conclusion can be drawn for the RD reconstruction. If we want $R(x; \bar{w})$ to satisfy (2), the stencil of points

selected by the ENO interpolation must lie in the same region of smoothness of w.

We shall describe now the original Subcell Resolution technique due to Harten [5]. The basic idea is a simple one: In one dimension, the sliding average in a cell gives accurate information on the location of a discontinuity within that cell. An ENO reconstruction can, thus, be modified to account for discontinuities within the computational cells. Harten identifies a cell with a possible discontinuity in its interior as one for which the stencils assigned to its left and right neighbors are disjoint,

$$S_{r(j-1)} \cap S_{r(j+1)} = \emptyset.$$

In this case, we extend the reconstructions from the cells to the left and to the right, R_{j-1} and R_{j+1} into the j-th cell up to a point θ_j so that

$$F_j(\theta_j) = 0 \tag{6}$$

where

$$F_j(x) = \int_{x_{j-\frac{1}{2}}}^{x} R_{j-1}(\xi, v^n)d\xi + \int_{x}^{x_{j+\frac{1}{2}}} R_{j+1}(\xi, v^n)d\xi - h\bar{w}_j^n. \tag{7}$$

This will be possible if

$$F_j(x_{j-\frac{1}{2}}) \cdot F_j(x_{j+\frac{1}{2}}) \leq 0,$$

in this case, the reconstruction in the j-th cell is redefined as

$$\hat{R}(x, \bar{w}^n) = \begin{cases} R_{j-1}(x) & x_{j-\frac{1}{2}} \leq x \leq \theta_j \\ R_{j+1}(x) & \theta_j \leq x \leq x_{j-\frac{1}{2}}. \end{cases} \tag{8}$$

In order to evaluate $\hat{R}(x, \bar{w}^n)$ in (8) we do not have to know the exact location of the root θ_j, only whether $x < \theta_j$ or $x > \theta_j$. Assuming a single root in I_j, this can be accomplished by comparing the sign of $F_j(x)$ to that of the endpoints.Thus

$$\hat{R}(x, \bar{w}^n) = \begin{cases} R_{j-1}(x) & F_j(x_{j-\frac{1}{2}}) \cdot F_j(x) > 0 \\ R_{j+1}(x) & F_j(x) \cdot F_j(x_{j+\frac{1}{2}}) > 0. \end{cases}$$

The actual flux calculation in [5] is quite cumbersome. Using conservation in a clever way, Harten has devised a much simpler procedure to compute

the numerical flux. The derivation, unpublished until now, is given by Ami Harten in an Appendix to this paper.

As we will see later, in the case of a jump discontinuity, the ENO technique picks a one sided stencil when reconstructing at each side of the jump, therefore, the interpolating polynomial uses information from only one of the smooth sides of the solution. When the reconstructions to the left and to the right of the cell harboring the discontinuity are extended to that cell, we do get an accurate approximation of the solution. On the other hand, our numerical experiments reveal that, when dealing with a corner, the ENO technique might still pick information from across the corner in reconstructing the solution at the cells next to the one that contains it.

The ENO interpolatory technique was studied in detail in [6]. The authors show there that the interpolating polynomial will be monotone in a cell that contains a discontinuity of H in its interior. However, when applying the technique to solve a conservation law, we interpolate a function which is one degree smoother than the solution to the partial differential equation . Therefore jumps in u become corners for the function to be interpolated, and the monotonicity result does not apply. In any case, the success of the SR technique is not based on the properties of the reconstruction in cells that contain singularities, but in cells *next* to the one with the singularity.

We can conclude, then, that the success of the SR technique depends solely on the ability of the interpolatory technique to pick one sided stencils at the cells neighboring a singularity. In the next section, we investigate the spread of the error that a corner introduces in numerical approximations obtained via ENO schemes, and show that SR, as it is, fails to keep the numerical approximation accurate around the corner.

3 Local accuracy around corners

When dealing with nonlinear schemes, the question of accumulation of error has to be analyzed primarily via computational experiments. To this end, and to get a grasp on the problem, we solve numerically the linear advection equation with continuous, piecewise smooth initial data,

$$\begin{aligned} u_t - u_x &= 0 \\ u(x,0) &= \begin{cases} -\sin(\frac{\pi}{2}x) & -1 \le x < 0 \\ \sin(\frac{\pi}{2}x) & 0 \le x \le 1, \end{cases} \end{aligned} \tag{9}$$

using second and third order ENO schemes. In Figure 1 we show the

x-coord.	| u40-ut |	| u80-ut |	numer. order	
-1.000	0.36778321E-04	0.74442122E-05	2.305	
-0.950	0.37901373E-04	0.79356944E-05	2.256	
-0.900	0.38806222E-04	0.83783951E-05	2.212	
-0.850	0.43950582E-04	0.87680826E-05	2.326	
-0.800	0.51609843E-04	0.91142530E-05	2.501	
-0.750	0.24141219E-04	0.93470166E-05	1.369	
-0.700	0.66175473E-04	0.95982658E-05	2.785	
-0.650	0.94072660E-05	0.11994544E-04	-0.351	
-0.600	0.94600794E-03	0.87521738E-05	6.756	
-0.550	0.57520062E-02	0.61720144E-04	6.542	
-0.500	0.11853433E-01	0.20054690E-02	2.563	
-0.450	0.47713198E-03	0.71858019E-02	-3.913	
-0.400	0.32952060E-01	0.21142133E-01	0.640	– location of corner .
-0.350	0.67517649E-03	0.53464550E-02	-2.985	
-0.300	0.97776380E-02	0.14087049E-02	2.795	
-0.250	0.41747724E-02	0.24058211E-04	7.439	
-0.200	0.52785419E-03	0.19262944E-04	4.776	
-0.150	0.10696189E-03	0.64592174E-05	4.050	
-0.100	0.88795438E-04	0.78364293E-05	3.502	
-0.050	0.19559739E-04	0.70987159E-05	1.462	
0.000	0.14475275E-04	0.65594226E-05	1.142	
0.050	0.18802878E-04	0.59522417E-05	1.659	
0.100	0.15563837E-04	0.53116037E-05	1.551	
0.150	0.11762217E-04	0.46378442E-05	1.343	
0.200	0.86518550E-05	0.39355268E-05	1.136	
0.250	0.54034343E-05	0.32089448E-05	0.752	
0.300	0.20717014E-05	0.24625650E-05	-0.249	
0.350	0.12597829E-05	0.17010887E-05	-0.433	
0.400	0.45318902E-05	0.92882123E-06	2.287	
0.450	0.77417858E-05	0.15052637E-06	5.685	
0.500	0.10960447E-04	0.61790480E-06	4.149	
0.550	0.14711256E-04	0.14366108E-05	3.356	
0.600	0.17945143E-04	0.22256827E-05	3.011	
0.650	0.19866165E-04	0.28530570E-05	2.800	
0.700	0.22797052E-04	0.36586195E-05	2.639	
0.750	0.25820094E-04	0.43694170E-05	2.563	
0.800	0.28442211E-04	0.50534813E-05	2.493	
0.850	0.30807508E-04	0.57078838E-05	2.432	
0.900	0.32970342E-04	0.63268460E-05	2.382	
0.950	0.34982270E-04	0.69068201E-05	2.341	

Table 1: ENO2. Discontinous derivative.

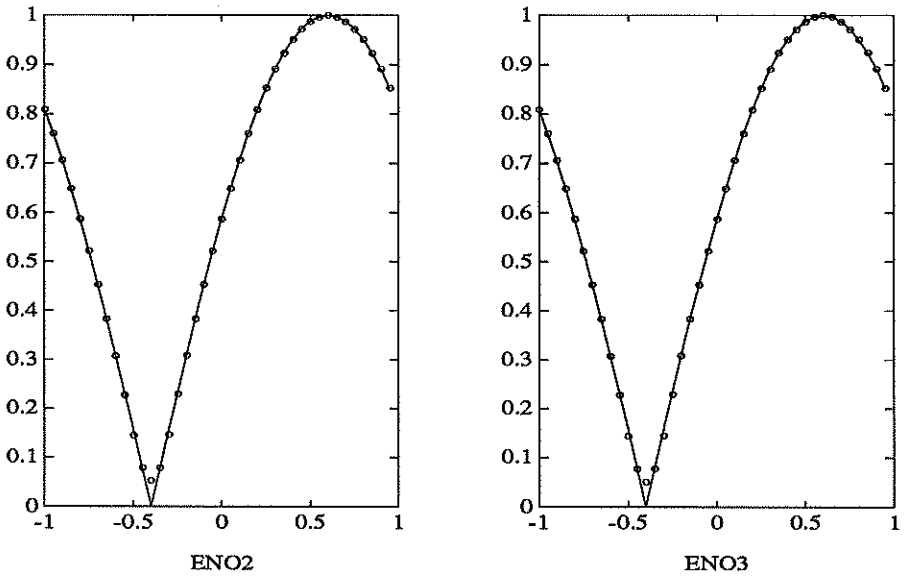

Figure 1: Initial data with discontinuous derivative

numerical solutions at time $t = .4$,. Table 1 shows errors and numerical orders (comparing with the true solution) for the second order method. When $h = 1/20$, the area of influence of the corner in the computation of the numerical solution is roughly $\approx [-.6, -.2]$. Comparing with data in [1], we see that the sizes of the polluted regions for corners are similar to those of jump discontinuities, although the pollution is certainly more dramatic in the case of a jump.

As we mentioned in the introduction, in the presence of coupling, the error spread caused by a corner can reduce the accuracy of the computed solution globally in large regions in the same manner a contact discontinuity did. We seek to remove these regions of low accuracy by reducing the error spread that the corner introduces in the computation.

It is obvious that an ENO reconstruction, smooth in the interior of each cell, cannot represent accurately the solution at a cell containing a corner. On the other hand, the basic principle underlying the SR technique :

Use the reconstructions at the cells next to the singularity to re-

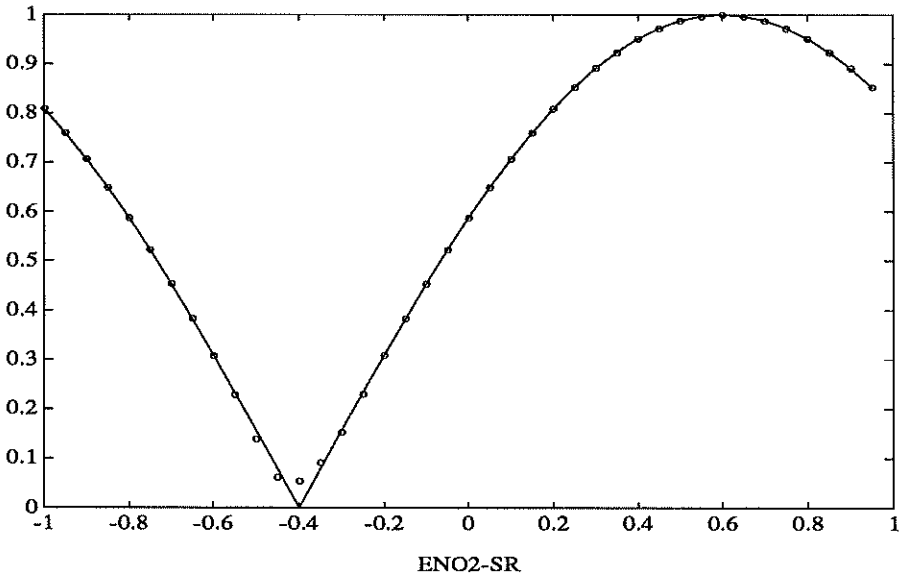

Figure 2: Unsuccesfull ENO2-SR

cover the singularity within the cell,

should work for corners just as well as it did for contact discontinuities. In order to confirm this observation, in our next experiment, we apply the SR technique to compute the solution of (9). For the time being, we ignore detection mechanisms and simply turn on the SR correction at the cell where the corner is located. This straight application of the technique gives unsatisfactory results. They are compiled in Table 2 for a second order method. We can see in the table and in figure 2, that the polluted region is of the same size as in the case of the plain ENO method.

The reason for the failure of the SR technique becomes apparent when we examine the stencils assigned to each computational cell by the ENO interpolatory technique. Subcell resolution relies heavily on the fact that the polynomial reconstructions from the cells to the left and to the right of the discontinuity represent the solution accurately. However, numerical experiments show that, when a corner is located in the interior of a cell I_j, the stencils selected by the ENO technique to construct $R_{j-1}(x)$ and $R_{j+1}(x)$ can

x-coord.	| u40-ut |	| u80-ut |	numer. order	
-1.000	0.36782313E-04	0.74442122E-05	2.305	
-0.950	0.37938204E-04	0.79356953E-05	2.257	
-0.900	0.38762450E-04	0.83783863E-05	2.210	
-0.850	0.43518546E-04	0.87681885E-05	2.311	
-0.800	0.51737141E-04	0.91131018E-05	2.505	
-0.750	0.28987203E-04	0.93572227E-05	1.631	
-0.700	0.59339187E-04	0.95365571E-05	2.637	
-0.650	0.44025456E-04	0.12112081E-04	1.862	
-0.600	0.68741694E-03	0.71778122E-05	6.581	
-0.550	0.49066815E-02	0.52822350E-04	6.537	
-0.500	0.17820093E-01	0.22306300E-02	2.998	
-0.450	0.15889789E-01	0.18965571E-01	-0.255	
-0.400	0.34545650E-01	0.28150688E-01	0.295	– location of corner .
-0.350	0.12696976E-01	0.36803447E-02	1.787	
-0.300	0.39022649E-02	0.26818612E-02	0.541	
-0.250	0.34542038E-02	0.33026743E-04	6.709	
-0.200	0.49516875E-03	0.19134324E-04	4.694	
-0.150	0.11733596E-03	0.64375187E-05	4.188	
-0.100	0.87563937E-04	0.78465561E-05	3.480	
-0.050	0.18682640E-04	0.70975194E-05	1.396	
0.000	0.14423937E-04	0.65594837E-05	1.137	
0.050	0.18674082E-04	0.59522451E-05	1.650	
0.100	0.15601442E-04	0.53116036E-05	1.554	
0.150	0.11786959E-04	0.46378440E-05	1.346	
0.200	0.86421507E-05	0.39355268E-05	1.135	
0.250	0.54024979E-05	0.32089448E-05	0.752	
0.300	0.20730586E-05	0.24625650E-05	-0.248	
0.350	0.12602105E-05	0.17010886E-05	-0.433	
0.400	0.45318105E-05	0.92882114E-06	2.287	
0.450	0.77417960E-05	0.15052626E-06	5.685	
0.500	0.10960446E-04	0.61790494E-06	4.149	
0.550	0.14711256E-04	0.14366110E-05	3.356	
0.600	0.17945143E-04	0.22256828E-05	3.011	
0.650	0.19866165E-04	0.28530571E-05	2.800	
0.700	0.22797054E-04	0.36586196E-05	2.639	
0.750	0.25820082E-04	0.43694172E-05	2.563	
0.800	0.28442204E-04	0.50534814E-05	2.493	
0.850	0.30807728E-04	0.57078840E-05	2.432	
0.900	0.32970162E-04	0.63268461E-05	2.382	
0.950	0.34979258E-04	0.69068203E-05	2.340	

Table 2: ENO2-SR. Discontinous derivative.

contain points from across the corner, thus invalidating the accuracy of the reconstructions. The analysis of the stencil selection at the cells I_{j-1} and I_{j+1} will shed light on the correct procedure to obtain accurate reconstructions in these cells.

4 Analysis of the ENO stencil around singularities

Let us consider the ENO interpolation problem for a continuous piecewise smooth function $H(x)$. Assume that $H'(x)$ has a discontinuity at x_d, where $x_d \in I_0 = (x_{-\frac{1}{2}}, x_{\frac{1}{2}})$, and it is otherwise smooth.

The ENO parabolic interpolant for H in $I_{-1} = (x_{-\frac{3}{2}}, x_{-\frac{1}{2}})$ is constructed as follows [6]:

$$\begin{aligned} q_{-1}^{(2)}(x) &= H[x_{-\frac{1}{2}}] + H[x_{-\frac{3}{2}}, x_{-\frac{1}{2}}](x - x_{-\frac{1}{2}}) \\ &+ \bar{m}(H[x_{-\frac{5}{2}}, x_{-\frac{3}{2}}, x_{-\frac{1}{2}}], H[x_{-\frac{3}{2}}, x_{-\frac{1}{2}}, x_{\frac{1}{2}}])(x - x_{-\frac{1}{2}})(x - x_{-\frac{3}{2}}) \end{aligned}$$

where,

$$\begin{aligned} \bar{m}(x,y) &= x \qquad \text{if} \quad |x| \le |y| \\ \bar{m}(x,y) &= y \qquad \text{if} \quad |x| > |y| \end{aligned}$$

A Taylor expansion around x_d gives :

$$\begin{aligned} H[x_{-\frac{5}{2}}, x_{-\frac{3}{2}}, x_{-\frac{1}{2}}] &= \frac{1}{2}H''(x_d^-) + O(h) \\ H[x_{-\frac{3}{2}}, x_{-\frac{1}{2}}, x_{\frac{1}{2}}] &= \frac{1-\theta}{2h}\{H'(x_d^+) - H'(x_d^-)\} \\ &+ \frac{1}{4}\{H''(x_d^+)(1-\theta)^2 + H''(x_d^-)[(\theta+1)^2 - 2\theta^2]\} + O(h), \end{aligned}$$

where

$$x_d = x_{-\frac{1}{2}} + \theta h.$$

Thus, it is clear that

$$H'(x_d^+) \neq H'(x_d^-) \quad , \quad 1 - \theta = O(1)$$

imply

$$\begin{aligned} H[x_{-\frac{5}{2}}, x_{-\frac{3}{2}}, x_{-\frac{1}{2}}] &= O(1) \\ H[x_{-\frac{3}{2}}, x_{-\frac{1}{2}}, x_{\frac{1}{2}}] &= O(1/h) \end{aligned}$$

and the ENO technique will choose $\{x_{-\frac{5}{2}}, x_{-\frac{3}{2}}, x_{-\frac{1}{2}}\}$ as the stencil to form $q_{-1}^{(2)}(x)$. Information is only taken from one of the smooth sides of the function. A similar analysis shows that, to construct $q_1^{(2)}(x)$, the stencil stays to the right of x_d.

If $(1-\theta) = O(h)$, the error in the reconstruction might be as bad as $O(h)$. The fact that the error for the reconstruction in a cell next to one harboring some kind of discontinuity, might be as bad as $O(h)$ was pointed out in an example in [6], section 5. We must remark, as they did, that this is a somewhat pathological case (the discontinuity being within $O(h^2)$ of a grid point), and this particular source of trouble has not been observed in any of the numerical experiments performed.

If u has a jump discontinuity, we will interpolate its primitive function (RP) or its sliding-average (RD). Either of these two functions is one degree smoother than u, so they will have a corner at the location of the jump in u. Our analysis shows that the stencil in cells neighboring the discontinuity stays to one side of it, thus ensuring optimal accuracy for the reconstruction in these cells. The necessary conditions for the success of the SR technique are satisfied.

On the other hand, if u is continuous but u' has a discontinuity at x_d, $H(x)$ and $H'(x)$ (or $\bar{w}$ and $\bar{w}'$ for RD) are continuous at x_d. The above Taylor expansions would give:

$$H[x_{-\frac{5}{2}}, x_{-\frac{3}{2}}, x_{-\frac{1}{2}}] = \frac{1}{2}H''(x_d^-) + O(h) \tag{10}$$

$$\begin{aligned} H[x_{-\frac{3}{2}}, x_{-\frac{1}{2}}, x_{\frac{1}{2}}] &= \frac{1}{4}\{H''(x_d^+)(1-\theta)^2 + H''(x_d^-)[(\theta+1)^2 - 2\theta^2]\} \\ &+ O(h) \end{aligned} \tag{11}$$

It is now quite possible to pick stencils that include points on both sides of the singularity, as demonstrated by the following example:

Consider,

$$H(x) = \begin{cases} x^2 & x \le 0 \\ \frac{1}{2}x^2 & x > 0 \end{cases}$$

and let $x_j = (j - \frac{1}{2})h$. Then

$$x_d = 0 \in (x_{-\frac{1}{2}}, x_{\frac{1}{2}}).$$

$H(x)$ has a discontinuity in its second derivative at $x = x_d = 0$, thus it would model the reconstruction problem for the primitive of a function with a corner at $x = 0$.

Substituting in (10) and (11), we get:

$$\begin{aligned} H[x_{-\frac{5}{2}}, x_{-\frac{3}{2}}, x_{-\frac{1}{2}}] &= 1 + O(h) \\ H[x_{-\frac{3}{2}}, x_{-\frac{1}{2}}, x_{\frac{1}{2}}] &= \frac{15}{16} + O(h). \end{aligned}$$

For sufficiently small h, $\{x_{-\frac{3}{2}}, x_{-\frac{1}{2}}, x_{\frac{1}{2}}\}$ would be the selected stencil for $q_{-1}^{(2)}(x)$. It is obvious that, with this choice, the accuracy of $q_{-1}^{(2)}(x)$ is at most $O(h)$.

The example shows why the SR technique is bound to fail when applied to recover the location of a corner with an underlying second order ENO scheme.

This scenario can be avoided for third and higher order reconstructions. The ENO interpolating cubic for H in I_j is as follows:

$$\begin{aligned} q_j^{(3)}(x) &= H[x_{i(j)}] + H[x_{i(j)}, x_{i(j)+1}](x - x_{i(j)}) \\ &+ H[x_{i(j)}, x_{i(j)+1}, x_{i(j)+2}](x - x_{i(j)})(x - x_{i(j)+1}) \\ &+ H[x_{i(j)}, x_{i(j)+1}, x_{i(j)+2}, x_{i(j)+3}](x - x_{i(j)})(x - x_{i(j)+1})(x - x_{i(j)+2}) \end{aligned}$$

where $x_{i(j)}$ is the first point in the 4-point stencil associated to the $j-th$ cell. For a given cell, the stencil can be chosen now in a *hierarchical* (Algorithm I) or a *non hierarchical* (Algorithm II) way. We describe these two algorithms in the general case.

Let $x_{i_k(j)}$ be the first point in the $k+1$-point stencil of points necessary to get a k-th order interpolating polynomial for H in the j-th cell, $(x_{j-\frac{1}{2}}, x_{j+\frac{1}{2}})$. Obviously, we take $x_{i_1(j)} = x_{j-\frac{1}{2}}$.

Algorithm I : Hierarchical choice of stencil.

Assume $i_k(j)$ given,

$$i_{k+1}(j) = \begin{cases} i_k(j) - 1 & \text{if} \quad \left|H[x_{i_k(j)-1}, \cdots, x_{i_k(j)+k}]\right| < \left|H[x_{i_k(j)}, \cdots, x_{i_k(j)+k+1}]\right| \\ i_k(j) & \text{otherwise} \end{cases}$$

Algorithm II : Non-Hierarchical choice of stencil.

Choose $i_k(j)$ so that

$$H[x_{i_k(j)}, \cdots, x_{i_k(j)+k}] = \min\{|H[x_l, \cdots, x_{l+k}]|, \quad j-k+\frac{1}{2} \le l \le j-\frac{1}{2}\}$$

For $k = 2$ both algorithms are the same.

In the example, we have shown that Algorithm I can lead to the *wrong* stencil at level $k = 2$. Since the stencil is calculated recursively, increasing the degree of the interpolating polynomial cannot improve the accuracy of the interpolant. However, Algorithm II determines the stencil by looking only at the highest divided difference of H, it bypasses the step $k = 2$ and is, thus, able to distinguish a corner in u (or discontinuity in H'').

Observe that:

$$\begin{aligned} H[x_{-\frac{5}{2}}, x_{-\frac{3}{2}}, x_{-\frac{1}{2}}, x_{\frac{1}{2}}] &= \frac{1-\theta}{2h}\{H''(x_d^+) - H''(x_d^-)\} + O(1) \\ H[x_{-\frac{7}{2}}, x_{-\frac{5}{2}}, x_{-\frac{3}{2}}, x_{-\frac{1}{2}}] &= \frac{1}{6}H'''(x_d^-) + O(h) \\ H[x_{-\frac{3}{2}}, x_{-\frac{1}{2}}, x_{\frac{1}{2}}, x_{\frac{3}{2}}] &= \frac{1+2\theta-2\theta^2}{12h}\{H''(x_d^+) - H''(x_d^-)\} + O(1) \end{aligned}$$

where H, u and x_d are as before.

Since $1 + 2\theta - 2\theta^2 > 1$, for $0 < \theta < 1$, Algorithm II would assign the stencil $\{x_{-\frac{7}{2}}, x_{-\frac{5}{2}}, x_{-\frac{3}{2}}, x_{-\frac{1}{2}}\}$ to the cell $(x_{-\frac{3}{2}}, x_{-\frac{1}{2}})$. Now, to construct the interpolant in this cell, we only take information from one of the smooth sides of the function, thus the requirements for the success of the SR technique are satisfied.

5 Modifying SR to sharpen corners

As we have seen in the previous section, if we intend to reduce the error spread introduced by a corner by using the SR technique, we must necessarily make use of third or higher order divided differences. Around a corner a non-hierarchical choice of stencil should be used to ensure a proper selection of the stencil.

We must point out though, that choosing the stencil in a non-hierarchical way consistently, leads to biased stencils. Algorithm II chooses the stencil according to the monotonicity properties of $H^{(k)}$, and its performance in the pre-asymptotic range is, in general, poorer that that of Algorithm II. In general, it is known that centered choices of stencil give better accuracy in the smooth range. For this reason, we have chosen to implement Algorithm I, except at the cells neighboring the singularity. This device, coupled with SR, gives excellent results, as proven by Table 3 and Figure 3. In Figure 3 the circles represent point values of u calculated using the reconstruction.

x-coord.	| u40-ut |	| u80-ut |	numer. order	
-1.000	0.13963885E-04	0.17287059E-05	3.014	
-0.950	0.13019776E-04	0.16242042E-05	3.003	
-0.900	0.12096651E-04	0.15096648E-05	3.002	
-0.850	0.11141306E-04	0.13858274E-05	3.007	
-0.800	0.99551450E-05	0.12534528E-05	2.990	
-0.750	0.81654569E-05	0.11125287E-05	2.876	
-0.700	0.65866961E-05	0.97611501E-06	2.754	
-0.650	0.11649528E-04	0.75046879E-06	3.956	
-0.600	0.35925869E-04	0.73675958E-06	5.608	
-0.550	0.26951611E-04	0.23998302E-05	3.489	
-0.500	0.10721541E-03	0.98231840E-05	3.448	
-0.450	0.79092848E-03	0.30049727E-04	4.718	
-0.400	0.15079518E-02	0.19591327E-03	2.944	– location of corner .
-0.350	0.82355897E-03	0.31757142E-04	4.697	
-0.300	0.14609759E-03	0.84240765E-05	4.116	
-0.250	0.10023506E-03	0.28713455E-05	5.126	
-0.200	0.49913546E-04	0.51578020E-06	6.597	
-0.150	0.96701252E-05	0.79715686E-06	3.601	
-0.100	0.13496128E-05	0.98803583E-06	0.450	
-0.050	0.81295045E-05	0.11230009E-05	2.856	
0.000	0.10753058E-04	0.12645054E-05	3.088	
0.050	0.11433245E-04	0.13959735E-05	3.034	
0.100	0.12166279E-04	0.15191341E-05	3.002	
0.150	0.13167218E-04	0.16328952E-05	3.011	
0.200	0.14064885E-04	0.17365915E-05	3.018	
0.250	0.14695076E-04	0.18296301E-05	3.006	
0.300	0.14684537E-04	0.19106404E-05	2.942	
0.350	0.14996517E-04	0.19860165E-05	2.917	
0.400	0.19934748E-04	0.20275422E-05	3.297	
0.450	0.31850687E-04	0.19627118E-05	4.020	
0.500	0.33924355E-04	0.30482060E-05	3.476	
0.550	0.30185995E-04	0.33899539E-05	3.155	
0.600	0.21902798E-03	0.18840262E-04	3.539	
0.650	0.38767237E-04	0.34493728E-05	3.490	
0.700	0.33104961E-04	0.30673358E-05	3.432	
0.750	0.33481730E-04	0.19162179E-05	4.127	
0.800	0.19930528E-04	0.20353110E-05	3.292	
0.850	0.14499142E-04	0.19800383E-05	2.872	
0.900	0.14486354E-04	0.19043163E-05	2.927	
0.950	0.14677536E-04	0.18227263E-05	3.009	

Table 3: ENO3-SR. Discontinous derivative.

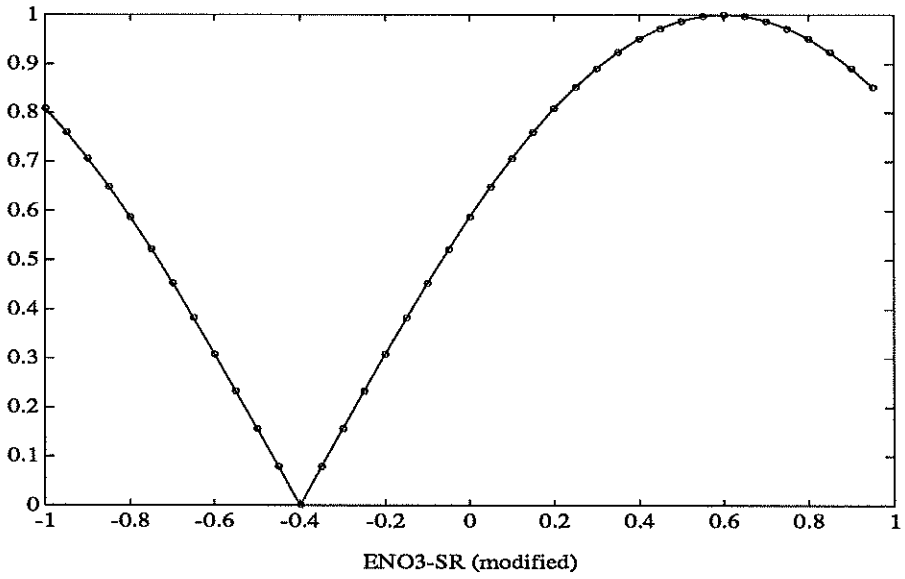

Figure 3: Initial data with discontinuous derivative

The strategy is as follows:

1. Sweep through the computational domain and calculate the ENO reconstruction at each cell using Algorithm I.

2. Use these reconstructions to single out cells suspected of harboring corners.

Remark: The detection algorithm proposed by Harten to identify a cell with a jump in its interior, uses the fact that, for a cell harboring a discontinuity

$$F_j(x_{j-\frac{1}{2}}) \cdot F_j(x_{j+\frac{1}{2}}) \leq 0, \tag{12}$$

where $F_j(z)$ is defined in (7) However, (12) does not hold at a cell containing a corner; in fact, if $w(x)$ is a piecewise polynomial function with discontinuous derivative at $\theta_j \in I_j$, then $F_j(\theta_j) = F_j'(\theta_j) = 0$. As it turns out, θ_j is an extremum of $F_j(x)$. We give a complete description of the detection technique in the next section.

3. Recompute the reconstructions at the two cells neighboring a cell with a corner using Algorithm II.

4. At each cell suspected of having a corner, modify the ENO reconstruction via Subcell Resolution, that is, extend the reconstructions to the left and to the right of the candidate cell to the computed location of the corner inside it.

Note: As in the original SR technique, it is not necessary to compute the location of the corner to proceed.

Table 5 shows that this simple procedure eliminates the error spread introduced in the computation by the corner.

6 Subcell Resolution for corners

In this section we show how to modify an ENO reconstruction so as to allow for the recovery of corners in the interior of the cells. To illustrate the procedure, we first consider a continuous piecewise polynomial function $w(x)$ of the form

$$w(x) = \begin{cases} P_L(x) & x < x_d \\ P_R(x) & x > x_d \end{cases}$$

$$P_L(x_d) = P_R(x_d); \qquad P_L{}'(x_d) \neq P_R'(x_d), \tag{13}$$

and we assume that the singularity is located in the interior of the interval I_0

$$x_{-1/2} < x_d < x_{1/2}.$$

Consider $R(x)$ an ENO reconstruction of $w(x)$. Provided that the stencils assigned to cells I_j, $j \neq 0$ are selected from the smooth part of the function, we have that

$$\begin{array}{rcl} R_j(x) = P_L(x) + O(h^r) & & j \leq -1 \\ R_j(x) = P_R(x) + O(h^r) & & j \geq 1. \end{array} \tag{14}$$

Where $R_j(x)$ is the polynomial defining $R(x)$ in I_j. Obviously, $R_0(x)$ cannot be an accurate approximation of w in I_0.

Using (13) and (14), we can modify $R(x)$ in I_0 as follows: Extend $R_{-1}(x)$ to a point z in I_0 from the left and $R_1(x)$ to z from the right, and approximate the location of the corner in I_0 by finding a value of z that satisfies

$$G_0(z) = R_{-1}(z) - R_1(z) = 0.$$

When h is sufficiently small, we expect to have

$$G_0(x_{-1/2}) \cdot G_0(x_{+1/2}) \leq 0,$$

and a single root of $G_0(z) = 0$ in I_0; we denote this root by θ_0

$$G_0(\theta_0) = 0.$$

It follows from (14) that

$$|\theta_0 - x_d| = O(h^r).$$

The *ENO reconstruction with subcell resolution*, $\hat{R}(x)$, is the following:

$$\begin{aligned} \hat{R}(x) &= R_j(x) && x \in I_j, \quad j \neq 0 \\ \hat{R}(x) &= \begin{cases} R_{-1}(x) & x_{-1/2} < x < \theta_0 \\ R_1(x) & \theta_0 < x < x_{1/2} \end{cases} && x \in I_0. \end{aligned}$$

As in Harten's subcell resolution, if the polynomial degrees of P_L and P_R are less than or equal to r, we will have $\hat{R}(x) = w(x)$.

We turn now to describe the algorithm for a general continuous, piecewise smooth function $w(x)$. As in the previous case, we take $\hat{R}(x)$ on I_j to be $R_j(x)$ unless I_j is suspected of having a corner of $w(x)$ in its interior. In this case, we define

$$G_j(x) = R_{j-1}(x) - R_{j+1}(x) \tag{15}$$

and check whether

$$G_j(x_{j-\frac{1}{2}}) \cdot G_j(x_{j+\frac{1}{2}}) \leq 0. \tag{16}$$

If this holds, then there is a root $z = \theta_j$

$$G_j(\theta_j) = 0, \qquad x_{j-\frac{1}{2}} \leq \theta_j \leq x_{j+\frac{1}{2}} \tag{17}$$

and we define $\hat{R}(x)$ in the cell I_j as

$$\hat{R}(x) = \begin{cases} R_{j-1}(x) & x_{j-\frac{1}{2}} \leq x \leq \theta_j \\ R_{j+1}(x) & \theta_j \leq x \leq x_{j-\frac{1}{2}}. \end{cases}$$

If (16) does not hold, we take $\hat{R}(x) = R_j(x)$, $x \in I_j$.

The only thing which is left open at this point is the criterion to determine whether a cell is *suspected* of harboring a corner. We shall make use of the insight we gained last section, analyzing the choice of the stencil in cells neighboring the corner.

In the RP framework, we observed that, if w has a corner in $I_j = (x_{j-\frac{1}{2}}, x_{j+\frac{1}{2}})$, then its primitive function $H(x) = \int^x w(z)\,dz$ satisfies

$$\begin{aligned}
H[x_{j-\frac{7}{2}}, x_{j-\frac{5}{2}}, x_{j-\frac{3}{2}}, x_{j-\frac{1}{2}}] &= O(1) \\
H[x_{j-\frac{5}{2}}, x_{j-\frac{3}{2}}, x_{j-\frac{1}{2}}, x_{j+\frac{1}{2}}] &= O(1/h) \\
H[x_{j-\frac{3}{2}}, x_{j-\frac{1}{2}}, x_{j+\frac{1}{2}}, x_{j+\frac{3}{2}}] &= O(1/h) \\
H[x_{j-\frac{1}{2}}, x_{j+\frac{1}{2}}, x_{j+\frac{3}{2}}, x_{j+\frac{5}{2}}] &= O(1/h) \\
H[x_{j+\frac{1}{2}}, x_{j+\frac{3}{2}}, x_{j+\frac{5}{2}}, x_{j+\frac{7}{2}}] &= O(1)
\end{aligned}$$

Since

$$H[x_{j-k-\frac{1}{2}}, \cdots, x_{j+\frac{1}{2}}] = \frac{1}{k+1}\bar{w}[x_{j-k}, \cdots, x_j],$$

the detection algorithm we propose is as follows:

Define

$$\begin{aligned}
ds &:= \min(|\bar{w}[x_{j-2}, x_{j-1}, x_j]|, |\bar{w}[x_{j-1}, x_j, x_{j+1}]|, |\bar{w}[x_j, x_{j+1}, x_{j+2}]|) \\
db &:= \max(|\bar{w}[x_{j-3}, x_{j-2}, x_{j-1}]|, |\bar{w}[x_{j+1}, x_{j+2}, x_{j+3}]|)
\end{aligned}$$

If

$$ds > db \tag{18}$$

and

$$G_j(x_{j-\frac{1}{2}}) \cdot G_j(x_{j+\frac{1}{2}}) \leq 0. \tag{19}$$

then

$$\hat{R}(x) = \begin{cases} R_{j-1}(x) & x_{j-\frac{1}{2}} \leq x \leq \theta_j \\ R_{j+1}(x) & \theta_j \leq x \leq x_{j-\frac{1}{2}}. \end{cases}$$

where

$$G_j(\theta_j) = 0.$$

Otherwise,

$$\hat{R}(x) = R_j(x) \quad x \in I_j.$$

Remark 1 . As stated, the algorithm may correct the ENO reconstruction at isolated cells where the solution is actually smooth. However, because of the smoothness of $w(x)$ there, we have

$$R_{j\pm1}(x) = w(x) + O(h^r), \qquad x \in I_j$$

consequently the error is still of the size of the reconstruction error.

Remark 2. We prove

$$|\theta_0 - x_d| = O(h^r)$$

as follows: Let us define $G(z) := P_L(z) - P_R(z)$, then

$$G_0(z) = R_{-1}(z) - R_1(z) = P_L(z) - P_R(z) + O(h^r) = G(z) + O(h^r)$$

therefore,

$$0 = G_0(\theta_0) = G(\theta_0) + O(h^r) = G(x_d) + (x_d - \theta_0)G'(x_d) + \cdots + O(h^r).$$

Since $|\theta_0 - x_d|$ is at least $O(h)$, $G(x_d) = 0$ and $G'(x_d) \neq 0$, we must have

$$|\theta_0 - x_d| = O(h^r).$$

It is easy to see now that

$$F_0(\theta_0) = O(h^r) \tag{20}$$

Remark 3. Recall that when reconstructing via a hierarchical algorithm, we must recalculate the reconstruction in the two cells neighboring a cell I_j in which (18) is satisfied, before we check (19). This ensures the accuracy of R_{j-1} and R_{j+1}, which is essential to determine θ_j accurately.

Remark 4. An ENO scheme based on cell averages can be written in conservation form due to a basic property of the reconstruction, namely

$$\bar{R}(x_j, \bar{w}) = \bar{w}_j.$$

Harten's SR-reconstruction preserves this property, i.e.

$$\bar{\hat{R}}(x_j; \bar{w}) = \bar{w}_j.$$

Instead, if x_d is a corner of $w(x)$ inside I_j, our SR-reconstruction satisfies:

$$\begin{aligned}
h\bar{\hat{R}}(x_j; \bar{w}) &= \int_{x_{j-\frac{1}{2}}}^{x_{j+\frac{1}{2}}} \hat{R}(x)\,dx \\
&= \int_{x_{j-\frac{1}{2}}}^{\theta_j} R_{j-1}(x) + \int_{\theta_j}^{x_{j+\frac{1}{2}}} R_{j+1}(x) \\
&= h\,\bar{w}_j + \int_{x_d}^{\theta_j} (R_{j-1}(x) - R_{j+1}(x))\,dx + O(h^{r+1}) \\
&= h\,\bar{w}_j + \int_{x_d}^{\theta_j} (x - x_d)\,(R'_{j-1}(x) - R'_{j+1}(x))\,dx + O(h^{r+1})
\end{aligned}$$

therefore

$$\bar{\tilde{R}}(x_j;\bar{w}) = \bar{w}_j + O(h^r). \tag{21}$$

In order to compute the numerical flux in the case of a corner within the j-th cell, one proceeds as in harten's SR. In fact the derivation carries through step by step, the only variations are due to (21) and (20), but these two modifications introduce terms that are on the order of the truncation error and do not spoil the accuracy of the calculation.

Unfortunately, it is not possible to derive a closed expression such as (31) for the numerical flux, but the basic idea underlying its derivation, still provides a selection process that avoids the explicit calculation of $x_s(\tau)$. In fact, the location of the corner at time τ will satisfy an equation similar to (17). We must have

$$\tilde{G}_j(x_s(\tau)) = 0,$$

where

$$\tilde{G}_j(x) = \tilde{v}_{j-1}(x,\tau) - \tilde{v}_{j+1}(x,\tau).$$

To determine the location of $x_{j+\frac{1}{2}}$ with respect to $x_s(\tau)$ (assuming the corner moves to the right) one simply does the following:

$$\bar{f}_{j+\frac{1}{2}} = \begin{cases} \bar{f}^L_{j+\frac{1}{2}} & \text{if} \quad \tilde{G}_j(x_{j-\frac{1}{2}}) \cdot \tilde{G}_j(x_{j+\frac{1}{2}}) > 0 \\ \bar{f}^R_{j+\frac{1}{2}} & \text{otherwise} \end{cases}$$

where $\bar{f}^L_{j+\frac{1}{2}}$ and $\bar{f}^L_{j+\frac{1}{2}}$ are as defined in (29), (30). If the discontinuity moves to the left, one has to determine the location of $x_{j-\frac{1}{2}}$ with respect to $x_s(\tau)$.

7 Subcell Resolution and Rarefaction corners. Limitations and Conclusions

We would like to show now that, with a little care, the techniques described in the last two sections can also be applied to sharpen the corners of rarefaction wave solutions of nonlinear equations and systems.

We start with the standard example of a single scalar nonlinear conservation
law : Burgers' equation. We attempt to compute the solution of

$$\begin{aligned} u_t + (u^2/2)_x &= 0 \\ u(x,0) &= \begin{cases} -1 & x < 0 \\ 1 & x > 0. \end{cases} \end{aligned} \tag{22}$$

The solution is a centered rarefaction wave:

$$u(x,t) = \begin{cases} -1 & x < -t \\ x/t & -t < x < t \\ 1 & t < x \end{cases} \tag{23}$$

At the creation of a rarefaction wave, the two corners are so close together that the region of smoothness between the two is not wide enough to contain the stencil of points necessary for a reconstruction, therefore SR, as stated, does not have a chance to succeed. In fact, Sever [12] has shown that, because of its self-similar nature, the rate of convergence of any numerical scheme approximating (22) is inherently limited to first order.

To avoid this conflict, we will consider instead

$$\begin{aligned} u_t + (u^2/2)_x &= 0 \\ u(x,0) &= \begin{cases} -1 & x < -\alpha \\ x/\alpha & -\alpha < x < \alpha \\ 1 & \alpha < x \end{cases} \end{aligned} \tag{24}$$

for $0 < \alpha < 1$.

Figure 4 shows approximations to (24) with $\alpha = .6$, obtained with an ENO3 scheme and 20 points ($h = 6/20$) at $t = 1.2$ and with the SR-corrected version of the same scheme. As expected, SR eliminates the error spread introduced in the computation by the corners of the rarefaction wave.

We conclude by showing an example where we apply the corner-SR technique to compute accurately rarefaction wave solutions of a system of hyperbolic conservation laws.

The equations for isothermal flow

$$\begin{bmatrix} \rho \\ m \end{bmatrix}_t + \begin{bmatrix} m \\ \dfrac{m^2}{\rho} + a^2\rho \end{bmatrix}_x \tag{25}$$

provide a non-trivial example of a system of two conservation laws.

Figure 7 shows a numerical approximation to the solution of the isothermal equations with the following initial data:

$$\begin{pmatrix} \rho \\ m \end{pmatrix}(x,0) = \begin{cases} \begin{pmatrix} 1 \\ 0 \end{pmatrix} & x \leq -.2 \\ \begin{pmatrix} e^{-(5x+1)} \\ e^{-(5x+1)}(5x+1) \end{pmatrix} & -.2 < x < .2 \\ \begin{pmatrix} e^{-2} \\ 2e^{-2} \end{pmatrix} & x \geq -.2 \end{cases}$$

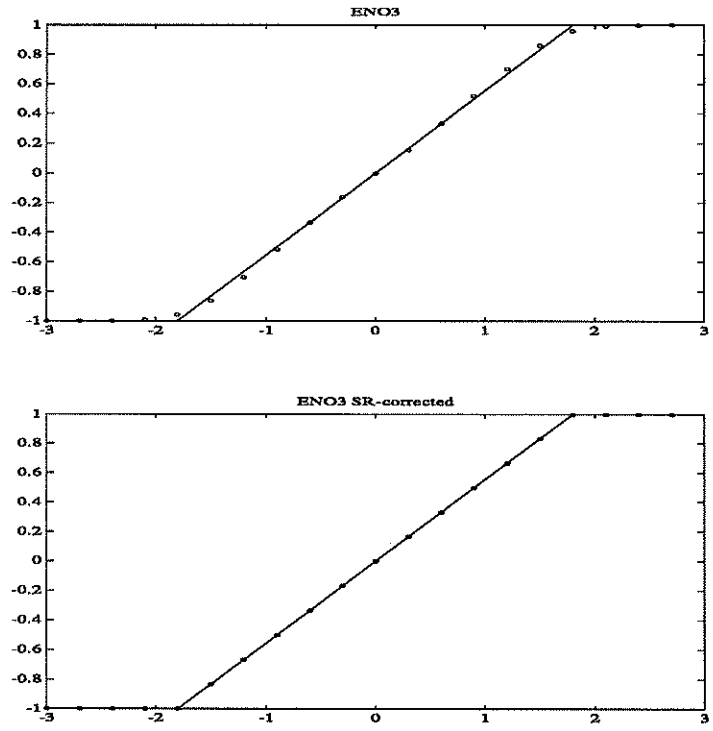

Figure 4: Rarefaction wave for Burgers' equation

obtained with a third order ENO scheme. We have used 40 points, or $h = 2/40$, and have run the scheme until $t = .2$, so the rarefaction corners are located at $x = \pm.4$. The dots represent values of the solution calculated using the reconstruction, and the solid line is the true solution, which in this case can be calculated explicitly.

We see that the corner SR technique is able to eliminate the spurious error spread associated to the computation of corners. However, the very nature of the technique makes it unsuitable for accurately representing rarefaction waves at their starting point. We need to be able to choose a stencil of points from the same side of smoothness of the solution function. This is not possible at the spring of a rarefaction wave.

Conclusions We have studied the behavior of ENO schemes for systems of Conservation Laws in one dimension, when the solution function exhibits discontinuities in its derivatives (*corners*). The analysis of the stencil selec-

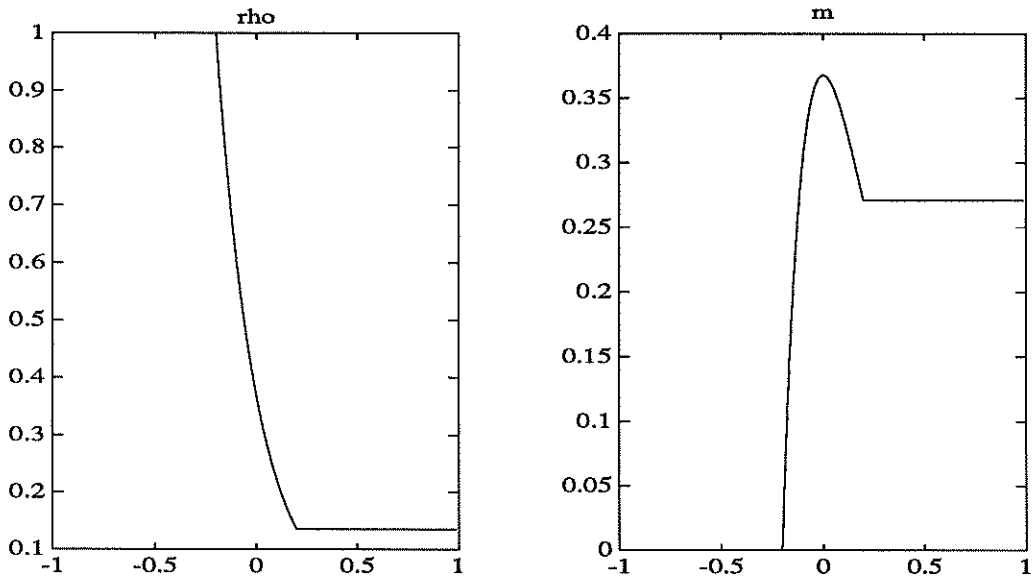

Figure 5: Initial values for isothermal system.

tion process allows us to identify the potential causes of error spread and loss of accuracy. This analysis also enables us to devise a subcell resolution mechanism that is able to keep the corners sharp when the computation proceeds. As stated, the correction is a one-dimensional technique.

We think that SR corrections for jump discontinuities are more natural in numerical approximations to solutions of conservation laws. This is supported by the fact that Harten's reconstruction is conservative while our reconstruction is conservative up to the level of the truncation error. Nevertheless, we think our study does contribute to a better understanding of the nonlinear process involved in ENO schemes.

Acknowledgements I would like to thank Ami Harten for his many suggestions and comments.

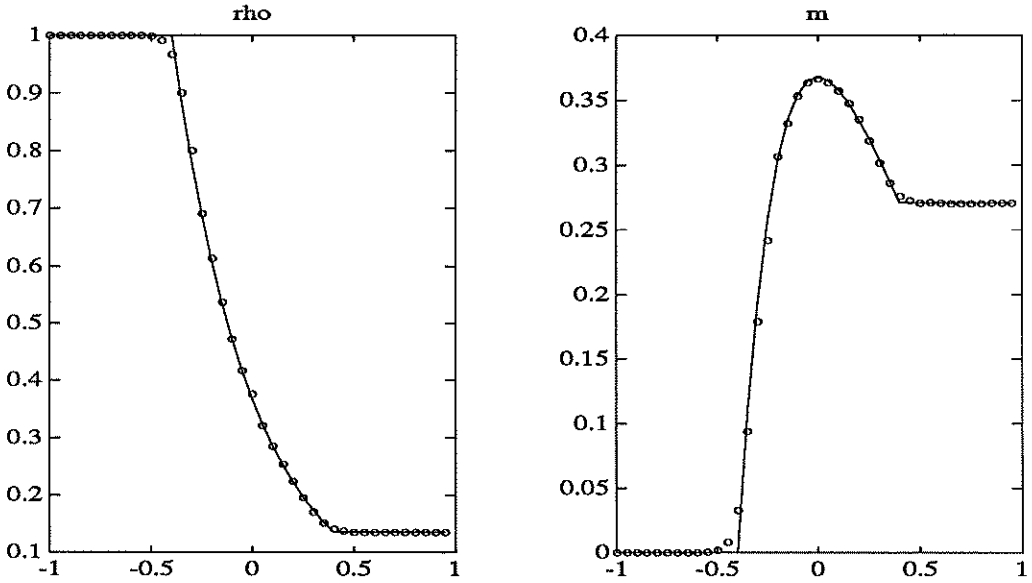

Figure 6: Third order method.

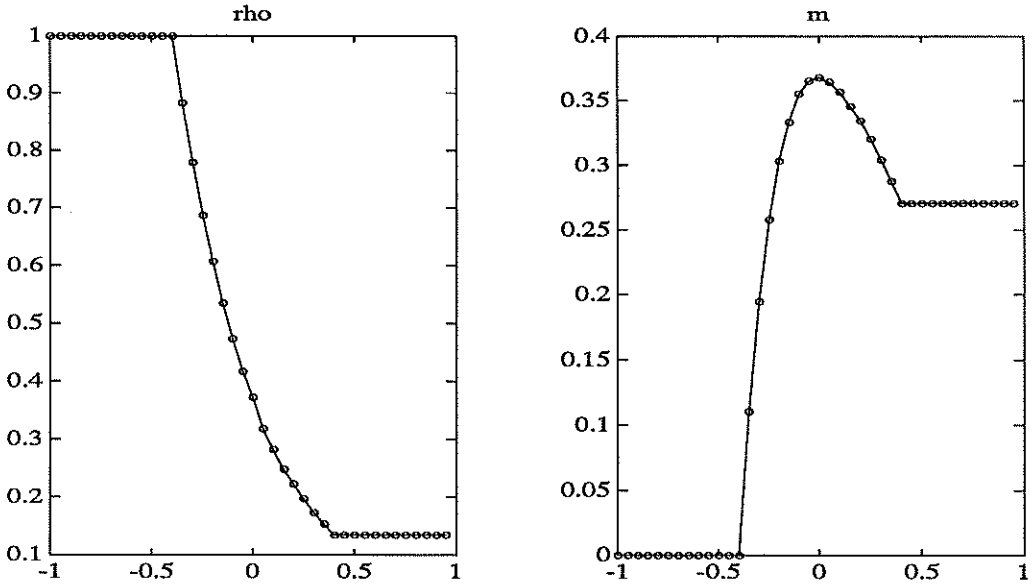

Figure 7: SR-corrected third order method.

APPENDIX
A. Harten

The purpose of this appendix is to show how to carry out the flux computation in the Subcell Resolution context when there is a discontinuity within the j-th cell. This derivation generalizes the procedure in [5] to the nonlinear case.

Let us assume that the discontinuity is propagating to the right, and denote its location by $x_s(t)$, with $x_s(0) = \theta_j$. Let us denote by $\tilde{v}_i(x,t)$ the solution of the IVP

$$u_t + f(u)_x = 0 \qquad u(x,0) = R_i(x, \bar{w}^n). \tag{26}$$

Since the initial data here are polynomial, the solution remains smooth for some time, and can be approximated in the small by a Taylor expansion. Under a suitable CFL restriction, the numerical flux of the Godunov-type scheme represented abstractly by (1) is given by

$$f_{j+\frac{1}{2}} = \frac{1}{\tau}\int_0^\tau f(v(x_{j+\frac{1}{2}}, t))dt$$

where $v(x,t)$ is the solution of

$$u_t + f(u)_x = 0 \qquad u(x,0) = \begin{cases} R_{j-1}(x, \bar{w}^n) & x < \theta_j \\ R_{j+1}(x, \bar{w}^n) & x > \theta_j \end{cases} \tag{27}$$

The solution to this problem can be expressed in terms of the solutions to the polynomial initial value problems (26) by

$$v(x,t) = \begin{cases} \tilde{v}_{j-1}(x,t) & x < x_s(t) \\ \tilde{v}_{j+1}(x,t) & x > x_s(t) \end{cases}.$$

First, let us consider the case $x_s(\tau) > x_{j+1/2}$; in this case $v(x,\tau) = \tilde{v}_{j-1}(x,\tau)$ for $x_{j-\frac{1}{2}} < x < x_{j+\frac{1}{2}}$, and the numerical flux can be found from considerations of conservation in the j-th cell. Integrating (27) and (26) over $I_j \times (0,\tau)$ and using that $F_j(x_s(0)) = 0$, we get

$$\int_{x_{j-\frac{1}{2}}}^{x_{j+\frac{1}{2}}} \tilde{v}_{j-1}(x,\tau)dx - h\bar{w}^n + \tau \cdot \bar{f}_{j+\frac{1}{2}} - \int_0^\tau \tilde{f}(v_{j-1}(x_{j-\frac{1}{2}}, t))dt = 0. \tag{28}$$

On the other hand, if we do the same for $\tilde{v}_{j-1}(x,t)$ in (26), we get

$$\begin{aligned}\int_{x_{j-\frac{1}{2}}}^{x_{j+\frac{1}{2}}} \tilde{v}_{j-1}(x,\tau)dx \;&-\; \int_{x_{j-\frac{1}{2}}}^{x_{j+\frac{1}{2}}} R_{j-1}(x,\bar{w}^n)dx \\ &+\; \int_0^\tau f(\tilde{v}_{j-1}(x_{j+\frac{1}{2}},t))dt - \int_0^\tau f(\tilde{v}_{j-1}(x_{j-\frac{1}{2}},t))dt = 0.\end{aligned}$$

Combining the last two equations and using the definition of $F_j(z)$, we can express the numerical flux in this case by

$$\begin{aligned}\tau\bar{f}_{j+\frac{1}{2}} &= \int_0^\tau f(\tilde{v}_{j-1}(x_{j+\frac{1}{2}},t))dt + h\bar{w}^n - \int_{x_{j-\frac{1}{2}}}^{x_{j+\frac{1}{2}}} R_{j-1}(x,\bar{w}^n)dx \\ &= \int_0^\tau f(\tilde{v}_{j-1}(x_{j+\frac{1}{2}},t)dt - F_j(x_{j+\frac{1}{2}}) =: \tau\bar{f}^L_{j+\frac{1}{2}}; \qquad (29)\end{aligned}$$

we denote this value by $\bar{f}^L_{j+\frac{1}{2}}$.

Next, we consider the case $x_s(\tau) < x_{j+\frac{1}{2}}$. Now $v(x_{j+\frac{1}{2}},t) = \tilde{v}_{j+1}(x_{j+\frac{1}{2}},t)$ for $0 \le t \le \tau$ and therefore the numerical flux is given by

$$\tau\bar{f}_{j+\frac{1}{2}} = \int_0^\tau f(\tilde{v}_{j+1}(x_{j+\frac{1}{2}},t)dt =: \tau\bar{f}^R_{j+\frac{1}{2}}. \qquad (30)$$

At this point, we have expressed the two possible values of the numerical flux in the case of a discontinuity propagating to the right

$$\bar{f}_{j+\frac{1}{2}} = \begin{cases} \bar{f}^L_{j+\frac{1}{2}} & \text{if} \quad x_s(\tau) > x_{j+\frac{1}{2}} \\ \bar{f}^R_{j+\frac{1}{2}} & \text{if} \quad x_s(\tau) < x_{j+\frac{1}{2}} \end{cases} \qquad (31)$$

in terms of solutions to the polynomial IVP (26), which can be approximated analytically to any desired accuracy ([6, 7]). The proper value to be used in (31) can be determined without having to compute the value of $x_s(\tau)$, provided the discontinuity is computationally meaningful. The main observation is that the location of the discontinuity at time τ satisfies an equation similar to (6), in fact

$$\tilde{F}_j(x_s(\tau)) = 0 \qquad (32)$$

where $\tilde{F}_j$ involves now the interval $(x_{j-\frac{1}{2}}, x_{j+\frac{3}{2}})$ at time τ and is defined as

$$\tilde{F}_j(x) = \int_{x_{j-\frac{1}{2}}}^{x} \tilde{v}_{j-1}(x,\tau)dx + \int_x^{x_{j+\frac{3}{2}}} \tilde{v}_{j+1}(x,\tau)dx - q_j^{n+1}, \qquad (33)$$

where

$$q_j^{n+1} = h(\bar{w}_j^n + \bar{w}_{j+1}^n) - \int_0^\tau f(\tilde{v}_{j+1}(x_{j+\frac{3}{2}}, t))dt + \int_0^\tau f(\tilde{v}_{j-1}(x_{j-\frac{1}{2}}, t))dt \quad (34)$$

Using (28),(29),(30) and the conservation relation for the solution of the polynomial IVP (26) in the $(j+1)$-th cell, we get

$$\tilde{F}_j(x_{j+\frac{1}{2}}) = \tau(\bar{f}_{j+1/2}^R - \bar{f}_{j+1/2}^L)$$

On the other hand, one can deduce directly from (32), (33), (34) that

$$\tilde{F}_j(x_{j+\frac{1}{2}}) = \tilde{F}_j(x_{j+\frac{1}{2}}) - \tilde{F}_j(x_s(\tau)) = \int_{x_{j-\frac{1}{2}}}^{x_{j+\frac{1}{2}}} [\tilde{v}_{j+1}(x,\tau) - \tilde{v}_{j-1}(x,\tau)]dx. \quad (35)$$

Equating the RHS of the last two equations and using the mean value theorem for the integral, we finally get

$$\tau(\bar{f}_{j+1/2}^R - \bar{f}_{j+1/2}^L) = [x_s(\tau) - x_{j+\frac{1}{2}}] \cdot (\tilde{v}^R - \tilde{v}^L) \quad (36)$$

where

$$(\tilde{v}^R - \tilde{v}^L) = [\tilde{v}_{j+1}(\psi,\tau) - \tilde{v}_{j-1}(\psi,\tau)], \qquad \psi \in (x_{j+\frac{1}{2}}, x_s(\tau)). \quad (37)$$

Multiplying (36) by

$$s = \mathrm{sgn}(\tilde{v}^R - \tilde{v}^L)$$

we find that

$$\mathrm{sgn}(s \cdot \bar{f}_{j+1/2}^R - s \cdot \bar{f}_{j+1/2}^L) = \mathrm{sgn}[x_s(\tau) - x_{j+\frac{1}{2}}]; \quad (38)$$

it follows that the numerical flux (31) can be expressed by

$$\bar{f}_{j+\frac{1}{2}} = s \cdot \min(s \cdot \bar{f}_{j+\frac{1}{2}}^L,\ s \cdot \bar{f}_{j+\frac{1}{2}}^R). \quad (39)$$

We recall that the evolution operator of the Conservation Law is order preserving; hence if $R_{j-1}(x, \bar{w}^n)$ and $R_{j+1}(x, \bar{w}^n)$ do not intersect in the interval I_j, then the respective solution in (37) keeps the same pointwise order. Consequently we can replace s in (37) by

$$s = \mathrm{sgn}(R_{j+1}(x_{j+\frac{1}{2}}, v^n) - R_{j-1}(x_{j+\frac{1}{2}}, v^n)).$$

The above assumption of nonintersection holds for any "computationally meaningful" discontinuity.

The numerical flux for the case of a discontinuity propagating to the right is given by (39) without any reference to the exact location of the discontinuity. A similar expression can be derived for the case of a discontinuity propagating to the left. If the initial discontinuity corresponds to a centered rarefaction wave, we do not use Subcell Resolution in this case.

References

[1] R. Donat, S. Osher, *Propagation of Error into Regions of Smoothness for Nonlinear Approximations to Hyperbolic Equations* Applied Mechanics and Engineering 80 (1990), pp. 59-64.

[2] S. K. Godunov, Math. Sb. 47 (1959),pp. 271-290; also: Cornell Aero. Lab. Transl.

[3] A. Harten, *The Artificial Compression Method for Computation of Shocks and Contact Discontinuities III. Self-Adjusting Hybrid Schemes.* Math. Comp. v.32 No. 142 (1978) pp. 363-389.

[4] A. Harten, *High Resolution Schemes for Hyperbolic Conservation Laws.* J. Comp. Physics, v. 49 (1983), pp. 357-393.

[5] A. Harten, *ENO schemes with Subcell Resolution,* J. Comp. Physics, v. 83 (1989), pp. 148-184; also ICASE Report # 87-56

[6] A. Harten, B. Engquist, S. Osher and S. Chakravarthy, *Some results on Uniformly High Order Accurate Essentially Non-oscillatory Schemes ,* Applied Numerical Mathematics No. 2, North-Holland, 1986, pp. 347-377.

[7] A. Harten, B. Engquist, S. Osher and S. Chakravarthy, *Uniformly High Order Accurate Essentially Non-oscillatory Schemes III,* J. Comp. Physics, v. 71 No. 2, (1987) pp. 231-303.

[8] A. Harten and S. Osher, *Uniformly High Order Accurate Nonoscillatory Schemes I,* SIAM Journal on Numerical Analysis, v. 24, No.2, (1987) pp. 279-309.

[9] A. Majda, J. McDonough and S. Osher, *The Fourier Method for Nonsmooth Initial Data,* Math. Comp. v. 32, (1978), pp. 1041-1081.

[10] A. Majda and S. Osher, *Propagation of error into regions of smoothness for Accurate Difference Approximations to Hyperbolic Equations,* Comm. Pure Appl. Math. 30, (1977), pp. 671-705.

[11] P. Lax, *Hyperbolic Systems of Conservation Laws and the mathematical theory of Shock Waves,* in ' Regional Conf. Series Lectures in Applied Math'. v. 11 SIAM, Philadelphia, 1972.

[12] M. Sever (Mock), *Order of dissipation near rarefaction centers,* in 'Progress and Supercomputing in Computational Fluid Dynamics, Proceedings of U.S.- Israel Workshop, 1984 Birkhauser, Boston, 1985, pp. 395

[13] C. W. Shu and S. J. Osher, *Efficient implementation of ENO schemes II.* J. Comp. Physics, v. 83 (1987) pp 439-471.

[14] H. Yang, *An Artificial Compression Method for ENO Schemes. The Slope Modification Method.* J. Comp. Physics, v. 89 (1990) pp 125-160.